2-1-2007

Threshold Power of Canonical Antennas for Inducing SAR at Compliance Limits in the 300-3000 MHz Frequency Range

Mohammod Ali
University of South Carolina - Columbia, alimo@engr.sc.edu

Mark G. Douglas
Motorola, Inc., mark.douglas@motorola.com

Abu T.M. Sayem
Motorola, Inc., abu.sayem@motorola.com

Antonio Faraone
Motorola, Inc., antonio.faraone@motorola.com

Chung-Kwang Chou
Motorola, Inc., ck.chou@motorola.com

Publication Info

Published in *IEEE Transactions on Electromagnetic Compatibility*, Volume 49, 2007, pages 143-152.
http://ieeexplore.ieee.org/xpl/RecentIssue.jsp?punumber=15

Threshold Power of Canonical Antennas for Inducing SAR at Compliance Limits in the 300–3000 MHz Frequency Range

Mohammod Ali, *Senior Member, IEEE*, Mark G. Douglas, *Senior Member, IEEE*, Abu T. M. Sayem, *Student Member, IEEE*, Antonio Faraone, *Senior Member, IEEE*, and Chung-Kwang Chou, *Fellow, IEEE*

***Abstract*—A study of the specific absorption rate (SAR) in an exposed body induced by canonical antennas is presented, with the aim of determining an upper bound for the antenna transmit power that demonstrates that a product is inherently compliant with internationally accepted radio frequency (RF) exposure limits. Starting from the fundamental limits in antenna quality factor (Q) and the corresponding bandwidth, several antenna sizes are selected, and their SAR distributions are computed using the method of moments (MoM) and finite-difference time domain (FDTD) method in the frequency range 300–3000 MHz. The threshold powers are then determined, below which the peak 1-g and 10-g averaged SAR would not exceed the limits specified in international exposure standards. From the data, simple expressions are derived to estimate the threshold power over a wide range of antenna sizes, frequencies, and distances from the body. It is demonstrated that the results presented in this paper are conservative in comparison with the measured SAR data of real products as well as other published data.**

***Index Terms*—Antennas, electromagnetic fields, electromagnetic propagation in absorbing media, finite difference methods, moment methods.**

I. Introduction

SPECIFIC absorption rate (SAR) is a metric of radio frequency (RF) energy exposure [1]. Proper evaluation of SAR for wireless transmitters is essential both in terms of compliance with RF exposure limits [2], [3] and antenna performance. SAR is measured using automated measurement systems in phantoms representing the human body [4], [5]. SAR can also be computed using various numerical electromagnetic modeling techniques, such as the finite-difference time domain (FDTD) method [6] and the method of moments (MoM) [7].

In the literature, there has been considerable research on mobile phone antennas and SAR [8]–[19]. Researchers have mainly been interested in the electromagnetic exposure of users from portable wireless devices and the influence of the user on the antenna performance in the 800–900 MHz and 1800–1900 MHz frequency bands. Most of the publications, to date, address different antenna types and their interaction with the human body, efficient numerical algorithms to compute SAR, and efficient antenna designs to reduce SAR. In contrast, this paper is an attempt to explore the relationship between SAR and antenna geometry for canonical antennas in the 300–3000 MHz frequency range with an aim to identify an upper bound of the transmitted power to meet a given SAR limit.

RF exposure standards address localized exposure to radio transmitters by limiting the peak mass-averaged SAR. For general public exposures at the head and torso, these limits are either 1.6 W/kg averaged over a 1-g mass (adopted in the United States of America, Bolivia, Canada, and South Korea) [2] or 2 W/kg averaged over a 10-g mass (adopted in 35 other countries, including Australia, Japan, and many European countries) [3]. The relationship between the peak SAR averaged over a mass m (denoted as SAR_m) and the root-mean-squared (rms) power transmitted by an antenna (P_t) can be described as

$$\mathrm{SAR}_m = \frac{P_m}{m} = \frac{1}{m}\frac{P_m}{P_{\mathrm{abs}}}\frac{P_{\mathrm{abs}}}{P_t}P_t = \frac{1}{m}F_m(1-\eta_{\mathrm{rad}})P_t \quad (1)$$

where P_m is the rms power absorbed in mass m, P_{abs} is the total rms power absorbed in the body, $F_m = P_m/P_{\mathrm{abs}}$ is an absorption factor representing the percentage of the absorbed power in the body that is dissipated in the averaging mass m, and $\eta_{\mathrm{rad}} = 1 - P_{\mathrm{abs}}/P_t$ is the radiation efficiency (i.e., the fraction of P_t that is not absorbed in the body).

The CENELEC EN 50371 standard provides a 20-mW threshold for the transmitted power above which SAR evaluation for compliance with the 2-W/kg SAR limit is needed [20]. Substituting $P_t = 20$ mW, $m = 10$ g, and $\mathrm{SAR}_{10\,\mathrm{g}} = 2$ W/kg in (1), it is seen that this threshold is conservative, as it is based on the assumption that all the power transmitted by the antenna is absorbed in the body (i.e., $\eta_{\mathrm{rad}} = 0$), making the device useless for communication, and all the absorbed power is concentrated in the 10-g mass (i.e., $F_{10\,\mathrm{g}} = 1$). However, in reality, $\eta_{\mathrm{rad}} > 0$ and $F_{10\,\mathrm{g}} < 1$; thus, the threshold power should be higher than 20 mW. Similarly, the threshold power ought to be higher than 1.6 mW for compliance with the IEEE C95.1-1991 standard.

The main objective of this paper is to analyze the relationship between SAR and antenna geometry, frequency, and bandwidth to determine suitable threshold power levels above which SAR evaluation must be done. Another objective is to derive a simple expression from the data that accurately estimates the threshold power from these parameters. It is important that the threshold power is conservative so that there is a negligibly low probability

Manuscript received February 10, 2006; revised September 4, 2006.

M. Ali and A. T. M. Sayem are with the University of South Carolina, Columbia, SC 29208 USA (e-mail: alimo@engr.sc.edu; sayem@engr.sc.edu).

M. G. Douglas, A. Faraone, and C.-K. Chou are with Motorola, Inc., Fort Lauderdale, FL 33322 USA (e-mail: mark.douglas@motorola.com; antonio.faraone@motorola.com; ck.chou@motorola.com).

Digital Object Identifier 10.1109/TEMC.2007.888178

that a portable wireless device with a transmit power below the threshold would induce a peak SAR exceeding the RF exposure limit. Although there are myriad mobile device geometries and body locations, we are interested in investigating relationships and trends of a general nature. Therefore, we consider canonical antennas (dipoles and loops) and a canonical body (a flat box phantom) over the considered frequency range. It will be shown that the phantom and antennas studied in this paper provide conservatively high SAR values for a given amount of emitted power compared to what would likely occur for a broad range of antenna types and portable wireless devices. In fact, earlier work by Okoniewski and Stuchly [9] showed that a flat phantom has a significantly higher SAR than that of a spherical or a realistic human head phantom. All considered antennas are lossless and perfectly matched. This ensures 100% antenna efficiency, so that the only losses are in the phantom, which also results in higher SAR values. At the end of the paper, a comparison is made between the results of this investigation and measured data from real portable wireless devices. The antennas studied can be regarded as representative of the radiation mechanisms characterizing a large majority of portable wireless devices. They may not be representative of highly directional antennas, such as those frequently employed in indoor/outdoor fixed transmitters, but such devices, which are not intended to operate near the user's head or body, are out of the scope of this paper.

II. Methodology

A. Numerical Modeling

SAR computations were conducted using commercial electromagnetic simulation codes based on FDTD (XFDTD v 6.3, Remcom Inc., State College, PA) [21] and MoM (FEKO Suite 4.3, EM Software & Systems-S.A. (Pty) Ltd., Stellenbosch, South Africa) [22]. Results using the two methods are checked against each other and against the measured and published data in Section III-A.

The setup used for all calculations consists of an antenna at a fixed distance from a flat phantom (see Fig. 1). The flat phantom consists of a lossy tissue equivalent material and a lossless phantom shell having a relative permittivity of 3.7. The dielectric parameters (ε_r, σ) and minimum dimensions (L, W, H) of the phantom material and the thickness (t) of the phantom shell meet the IEEE Std 1528-2003 specifications [4], which are reproduced in Table I. The phantom dielectric parameters were chosen to provide a conservatively high SAR in a homogeneous head model when compared to the heterogeneous case of a real person [4], [13]. The conservativeness of the phantom dielectric parameters has been verified independently [23], [24]. In addition, a current proposal [25] is to use these same dielectric parameters for the rest of the body. Thus, the results of this paper are applicable to both the head and the body of the user. The antenna is oriented in a plane parallel to the phantom shell with its center directly beneath the center of the phantom shell. The dipole antenna feed point is located between equal arms along the antenna axis. The antenna axis is spaced at a distance s from the interface between the phantom material and the phantom shell.

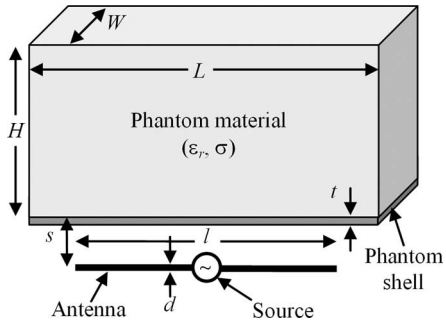

Fig. 1. Antenna and flat phantom setup. The variables are defined and specified in Table I.

TABLE I
Parameters of Flat Phantom and Dipole Antenna Setups

f (MHz)	ε_r	Phantom σ (S/m)	Phantom t (mm)	Phantom L, W (mm)	Dipole antenna l/λ	Dipole antenna d (mm)	Dipole antenna s (mm)
300	45.3	0.87	6.3	600, 400	0.396	6.35	15
450	43.5	0.87	6.3	400, 270	0.405	6.35	15
900	41.5	0.97	2	225, 150	0.447	3.6	15
1450	40.5	1.20	2	225, 150	0.431	3.6	10
1900	40.0	1.40	2	225, 150	0.431	3.6	10
2450	39.2	1.80	2	225, 150	0.421	3.6	10
3000	38.5	2.40	2	225, 150	0.415	3.6	10

The parameters are reproduced from [4]. For the phantom, ε_r and σ are the permittivity relative to air and the conductivity of the phantom liquid, respectively, t is the thickness of the lossless phantom shell which has a relative permittivity of 3.7 at all frequencies and L and W are the minimum phantom length and width (the minimum height H is always 150 mm). For the dipole antenna, l/λ is the length of the dipole relative to the wavelength in air, d is the diameter of the dipole and s is the distance of the dipole axis to the phantom liquid.

For the FDTD simulations, the voxel dimensions were kept below $\lambda/16$ in all directions and in all media. The uniform voxel dimensions were 1 mm for frequencies of 900 MHz and above and 1.5 mm for frequencies of 450 MHz and below. The FDTD model was bounded by perfectly matched layer (PML) absorbing boundaries with at least four layers. The absorbing boundaries were at a minimum distance of $\lambda_0/8$ from the model.

For the MoM simulations, Green's functions for planar multilayer dielectric media were chosen for the integral equations. To discretize and solve the integral equations, FEKO uses triangular expansion and testing functions for the wire models. The wire model segment length was less than $\lambda/15$ and at least 3.3 times the wire diameter.

In all cases, SAR averaging was carried out as prescribed by the IEEE Std C95.3-2002 [26].

B. Antenna Models

The purpose of this section is to define the antenna types and an appropriate range of antenna sizes for the study. Antenna sizes and types vary widely from one portable wireless device to another. For mobile transmitters, antennas can be broadly classified as external and internal antennas [27]. Examples of external antennas include whip and helical monopole antennas, while internal antennas include planar inverted-F antennas (PIFAs) [28]–[33] and folded inverted conformal antennas

(FICAs) [34]. This study focuses on two canonical antenna types, thin-wire dipoles and loops. The advantage of studying canonical antenna types is that it limits the number of variables to be studied while also representing the fundamental radiation mechanisms that characterize several broad classes of portable wireless devices, such as mobile phones and two-way portable radios and pagers. For example, only length and radius are varied with thin-wire dipoles, whereas with PIFAs, the size and shape of the patch element, the ground contact location, the feed location, and the size of the ground plane would all be variables in the investigation space. The applicability of the canonical antenna results to real portable wireless devices is addressed in Section III-C.

Since antenna size has a significant effect on SAR, it is important to determine the antenna sizes to be studied. The length of the dipole antennas will be varied from $\lambda/2$ to a minimum length. Dipole antennas longer than $\lambda/2$ are not of interest because the current distribution on such antennas has multiple peaks, resulting in lower peak mass-averaged SAR values for a given transmit power. Given that antenna size is related to bandwidth and that antennas for portable wireless devices must meet bandwidth requirements, it makes sense to use bandwidth specifications as the rationale for choosing the minimum length to be studied. The relationship between the size of an antenna and its maximum bandwidth (or minimum quality factor Q) has been studied extensively [35]–[39]. According to McLean [38], the minimum radiation Q of a lossless antenna that is contained within a sphere of radius a is given by

$$Q_{\min} = \frac{1}{(\beta a)^3} + \frac{1}{\beta a} \tag{2}$$

where $\beta = 2\pi/\lambda$. This equation is accurate for electrically small antennas, where $\beta a \leq 1$ [38]. For thin-wire dipole antennas, this corresponds to a length $l \approx 2a \leq \lambda/\pi$. The radiation Q is the ratio of stored to radiated energy of an antenna, and when Q is large, it is approximately equal to the inverse of the half-power bandwidth [40]. The half-power bandwidth corresponds approximately to a return loss of $|S_{11}| \leq -7$ dB [i.e., voltage standing wave ratio (VSWR) ≤ 2.6] for impedance matched antennas at resonance [41]. This bandwidth is denoted as $\mathrm{BW}_{7\,\mathrm{dB}}$ in this paper. In general, $\mathrm{BW}_{x\,\mathrm{dB}}$ will denote the fractional bandwidth over which $|S_{11}| \leq -x$ dB. Portable wireless devices are commonly designed to meet operating antenna bandwidths for $|S_{11}| \leq -9.5$ dB or -6 dB (corresponding to VSWR ≤ 2 or 3, respectively) rather than -7 dB. The fractional bandwidth is equal to 100% $\times \Delta f/f_0$, where $\Delta f = f_{\max} - f_{\min}$ and $f_0 = (f_{\min} + f_{\max})/2$, and where $f_{\min}$ and $f_{\max}$ are the lowest and highest frequencies over the range at which $|S_{11}| \leq -x$ dB. The values of $Q_{\min}$ and $\mathrm{BW}_{7\,\mathrm{dB}\,\max} = 1/Q_{\min}$ are given in Table II for a range of βa values.

In practice, there is no known antenna that achieves the upper bandwidth bounds in Table II, given the difficulty to utilize the spherical volume effectively [39]. Therefore, the bandwidths of practical antennas are significantly narrower than these bounds. Table III shows the fractional impedance bandwidths of dipole antennas calculated using MoM both in free space and near the flat phantom at three frequencies. None of these antennas are resonant by themselves, and thus, to calculate bandwidths, each antenna is made resonant by nullifying its reactance at the desired frequency (by inserting a lossless inductor in series with the capacitive reactance of the short antenna) and feeding it with a source matched to the antenna input resistance. Broadband matching networks can be used to achieve wider bandwidths at the expense of lower antenna efficiency due to circuit losses. For the results of Table III, the phantom parameters are as given in Table I, and the dipole antenna parameters are as shown in Table III. Results are shown at 300, 1450, and 3000 MHz, representing the lowest, middle, and highest frequencies studied.

TABLE II
Q AND BANDWIDTH LIMITS FOR ELECTRICALLY SMALL ANTENNAS

Antenna dimensions		Limits	
βa	l	Q_{min}	$BW_{7\mathrm{dB}\,max}$
0.2	λ/15.7	130	0.77%
0.4	λ/7.8	18	5.5%
0.6	λ/5.2	6.3	15.9%
0.8	λ/3.9	3.2	31.2%
1.0	λ/π	2	50.0%

TABLE III
CALCULATED FRACTIONAL IMPEDANCE BANDWIDTHS OF DIPOLE ANTENNAS

f (MHz)	300	300	1450	1450	1450	1450	3000
s (mm)	5	5	5	∞[1]	5	5	5
d (mm)	0.2	3.6	0.2	0.2	0.2	0.2	0.2
l	$BW_{6\mathrm{dB}}$	$BW_{6\mathrm{dB}}$	$BW_{6\mathrm{dB}}$	$BW_{7\mathrm{dB}}$	$BW_{7\mathrm{dB}}$	$BW_{9.5\mathrm{dB}}$	$BW_{6\mathrm{dB}}$
λ/15.7	0.7%	2.5%	0.2%	0.1%	0.2%	0.1%	0.1%
λ/7.8	1.9%	6.5%	1.0%	0.3%	0.8%	0.6%	0.6%
λ/5.2	4.0%	14%	2.4%	0.9%	2.1%	1.5%	1.6%
λ/3.9	7.2%	26%	4.7%	2.1%	4.1%	2.9%	3.5%
λ/π	11%	41%	8.0%	4.0%	6.9%	4.9%	5.9%

The phantom parameters are as given in Table I.
[1]A distance of $s = \infty$ means that the antenna is in free space (i.e., the phantom is not present).

The 7-dB bandwidths of the thin-wire dipoles in free space at 1450 MHz (see column 5 of Table III) can be compared with the McLean fundamental limits in Table II. The fractional bandwidths are about an order of magnitude narrower than those of the fundamental limits. As the dipoles are placed next to the phantom, the bandwidths increase significantly due to the introduction of losses in the near field that reduce the stored reactive energy of the antenna. At $s = 5$ mm (see column 6), $\mathrm{BW}_{7\,\mathrm{dB}}$ is approximately twice that for the same dipole antennas in free space. The other consequence of proximity to the phantom is degradation in antenna radiation efficiency. For instance, the radiation efficiency of the 1450-MHz dipole antenna with $s = 5$ mm and $l = \lambda/3.9$ is only 3%.

The fractional bandwidths are also shown at 1450 MHz for the practical cases of $|S_{11}| = -6$ dB and -9.5 dB (see columns 4 and 7 of Table III). The fractional bandwidths for $|S_{11}| = -6$ dB are also given at the lowest and highest frequencies studied for $s = 5$ mm (see columns 2 and 8 of Table III). The fractional bandwidth is widest at $f = 300$ MHz due to the fact that the antennas are electrically closest to the phantom, resulting in higher losses and lower radiation efficiency. Column 3 of Table III shows the influence of dipole diameter on bandwidth.

TABLE IV
SOME TYPICAL FREQUENCY BANDS OF PORTABLE WIRELESS DEVICES

f_{min} (MHz)	f_{max} (MHz)	BW	example air interface
385	400	3.8%	TETRA
410	430	4.8%	TETRA
450	520	14.4%	APCO
453	468	3.2%	GSM
806	870	7.6%	iDEN
810	958	16.7%	PDC
824	894	8.1%	IS-136
870	921	5.7%	TETRA
890	960	7.6%	GSM
896	940	4.8%	iDEN
1429	1501	4.9%	PDC
1710	1880	9.5%	GSM
1850	1990	7.3%	GSM
1920	2170	12.2%	UMTS
2300	2400	4.3%	WiBro
2400	2484	3.4%	Bluetooth

Frequency band usage depends on the spectrum allocation of each country (e.g., 1429-1501 MHz is used in Japan, 2300-2400 MHz in South Korea). Also, some of the frequency bands support more than one air interface. The air interface given above is one example.

At a dipole diameter of $d = 3.6$ mm (from Table I), $\mathrm{BW}_{6\,\mathrm{dB}}$ for 300 MHz dipole antennas next to the phantom is three to four times wider than those of the same dipole antennas with $d = 0.2$ mm. For this thicker dipole diameter, the tips of these dipole antennas do not fit completely inside the sphere of radius $2a$ described by McLean. This results in a slightly increased bandwidth, especially for the shorter antennas.

Finally, the operating bandwidths of the portable wireless devices operating at various frequency bands are listed in Table IV. Fractional bandwidths range from 3 to 17%. Since the bandwidths of the $\lambda/15.7$ dipole antennas in Table III are narrow compared to the bandwidths in Table IV, even when the antenna is as close as 5 mm from the lossy phantom material, it does not appear relevant to investigate the dipole antennas shorter than $\lambda/16$. Thus, our study focuses on studying the SAR resulting from canonical dipoles with lengths of $\lambda/16, \lambda/12, \lambda/8, \lambda/4$, and $\lambda/2$

III. RESULTS

A. Validation of Numerical Models for SAR

To verify the accuracy of the numerical models and to estimate the error of the results, the flat phantom and dipole antenna setup shown in Fig. 1 was simulated using MoM and FDTD. All SAR values are computed for an antenna transmit power of $P_t = 1$ W. In Table V, the peak 1-g and 10-g averaged SAR values from the MoM and FDTD simulations are compared with the reference values of IEEE Std 1528 [4]. The geometric and dielectric parameters of the setup were set as shown in Table I. The reference values are shown as SAR_m in units of Watts per kilogram, whereas the MoM and FDTD results are shown as $\Delta\mathrm{SAR}_m$, which is the percent change in SAR_m from the reference values. Table V also lists $\Delta\mathrm{SAR}_m$ for measurements that were conducted at the Motorola Corporate EME Research Laboratory, Fort Lauderdale, FL, on the same setup (except at 1450 and 3000 MHz, where dipole antennas conforming to the IEEE

TABLE V
COMPARISON OF MEASURED AND SIMULATED SAR DATA WITH IEEE 1528 REFERENCE SAR DATA USING THE SETUP PARAMETERS OF TABLE I

f (MHz)	SAR_{1g} / SAR_{10g} (W/kg) IEEE 1528	ΔSAR_{1g}/ ΔSAR_{10g} vs. IEEE 1528 Measured	MoM	FDTD
300	3.0 / 2.0	-6% / -6%	0% / 5%	7% / 5%
450	4.9 / 3.3	3% / 2%	-2% / 0%	2% / 0%
900	10.8 / 6.9	3% / 3%	-5% / -1%	3% / 4%
1450	29.0 / 16.0	-- / --	-3% / 2%	4% /6%
1900	39.7 / 20.5	4% / 5%	0% / 4%	4% / 5%
2450	52.4 / 24.0	3% / 5%	2% / 7%	0% / 3%
3000	63.8 / 25.7	-- / --	-2% / 4%	4% / 8%

SAR values are normalized to 1W of transmit power.

TABLE VI
COMPARISON OF SIMULATED SAR DATA AT $f = 900$ MHZ AND $s = 5$ MM

l	SAR_{1g} / SAR_{10g} (W/kg) MoM, $d = 3.6$ mm	ΔSAR_{1g}/ ΔSAR_{10g} vs. MoM FDTD, $d = 3.6$ mm	SAR_{1g} / SAR_{10g} (W/kg) MoM, $d = 0.2$ mm
λ / 16	125.5 / 46.3	10% / -1%	125.9 / 46.4
λ / 12	87.1 / 35.5	9% / 1%	87.2 / 35.5
λ / 8	53.2 / 26.5	7% / -1%	53.6 / 26.5
λ / 4	31.3 / 17.6	6% / -2%	31.3 / 17.8
λ / 2	14.2 / 8.0	2% / -9%	15.5 / 9.0

The parameters *s*, *d* and *l* of the setup are defined in Fig. 1. The values of other parameters (e.g., *t*, ε_r *and* σ) are given in Table I at *f* = 900 MHz. SAR values are normalized to 1W of transmit power.

Std 1528 specifications were not available) using the DASY4 system (Schmid & Partner Engineering AG, Zürich, Switzerland). The measured and simulated results are all within 8% of the reference values. Thus, the deviation of the measured values is always within the 11% measurement uncertainty (evaluated according to [4] for $k = 1$ standard deviations).

Table VI shows a comparison of MoM and FDTD results at 900 MHz using the setup of Fig. 1 and Table I, except that the antenna length is varied from $\lambda/2$ to $\lambda/16$, and a closer spacing of the dipole antenna axis to the liquid of $s = 5$ mm is used. The peak 1-g and 10-g averaged SAR values are given for the MoM results along with $\Delta\mathrm{SAR}_m$, which is the percent difference of the FDTD results from the MoM results. The two methods compare very well with each other, with a maximum deviation of 10%. The last column of Table VI shows the MoM results for the identical setup of column 2, except that $d = 0.2$ mm. The data show that changing the dipole diameter by more than an order of magnitude does not significantly affect the SAR, although, as discussed earlier, it does significantly affect the bandwidth. Therefore, the SAR results presented in the next section are expected to be stable over a wide range of practical wire radii (very thick dipole antennas could have different SAR values, but they are not of practical interest).

From the data in Tables V and VI, it is estimated that the maximum error of the calculations presented in this paper is of the order of 10%.

B. Threshold Power Results for Dipole Antennas

The SAR induced in a flat phantom by thin-wire dipole antennas was calculated using MoM with the setup of Fig. 1. The phantom dielectric parameters are specified in Table I across the

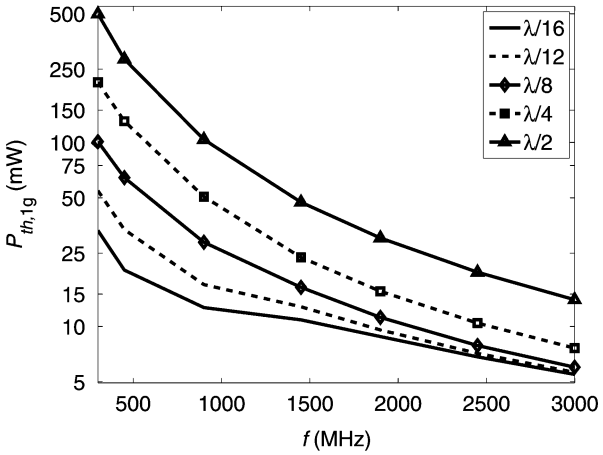

Fig. 2. Threshold power levels for $\mathrm{SAR}_{\mathrm{limit,1g}} = 1.6$ W/kg at $s = 5$ mm.

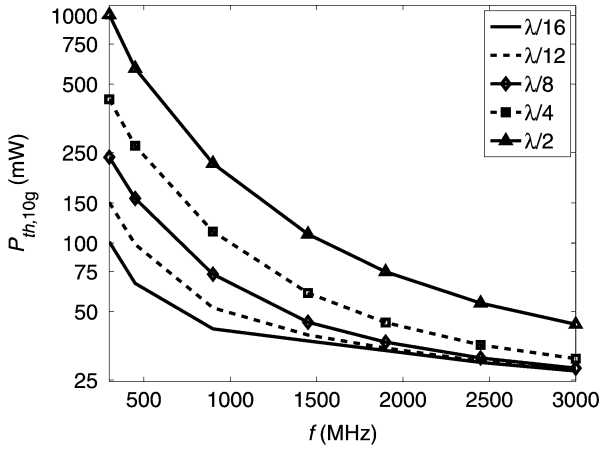

Fig. 3. Threshold power levels for $\mathrm{SAR}_{\mathrm{limit,10\,g}} = 2$ W/kg at $s = 5$ mm.

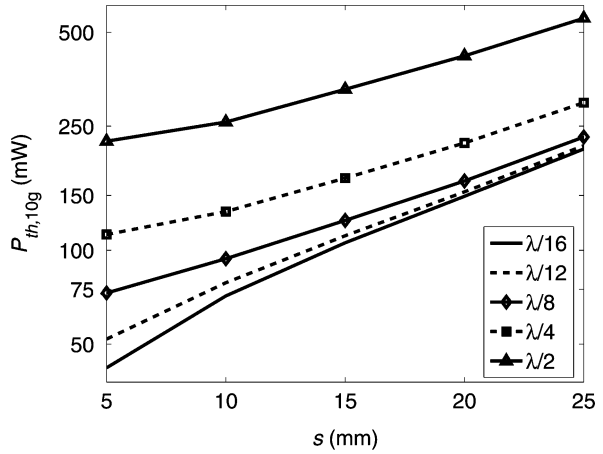

Fig. 4. Threshold power levels for $\mathrm{SAR}_{\mathrm{limit,10\,g}} = 2$ W/kg at $f = 900$ MHz.

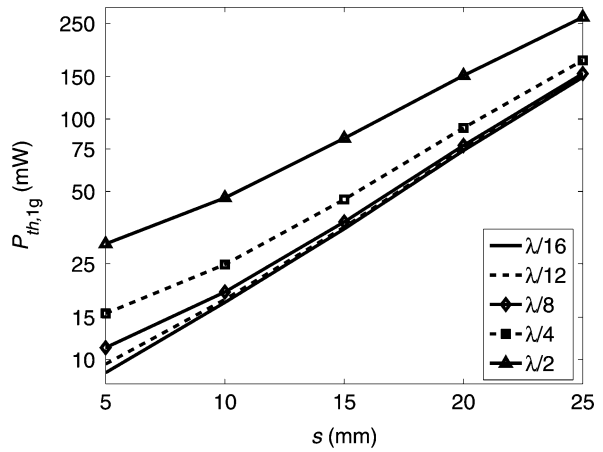

Fig. 5. Threshold power levels for $\mathrm{SAR}_{\mathrm{limit,1g}} = 1.6$ W/kg at $f = 1900$ MHz.

300–3000 MHz frequency range. The phantom shell thickness was fixed at 2 mm to allow the antennas to be spaced 5 mm from the phantom liquid. The dipole antennas have lengths of $l = \lambda/16, \lambda/12, \lambda/8, \lambda/4$, and $\lambda/2$ at each frequency and a constant diameter of $d = 0.2$ mm (i.e., not more than $\lambda/500$ at all frequencies). The segment length of the wire models was kept below $\lambda/100$. The dipole antenna was spaced away from the phantom at distances of $s = 5, 10, 15, 20$, and 25 mm, corresponding to the expected range of distances between the antenna of a portable wireless device and the user's body. Due to the 2-mm thickness of the phantom shell, the thickness of the plastic housing of a typical portable wireless device, and the spacing of the antenna away from the side of the device facing the body, a minimum distance of 5 mm was deemed reasonable. The largest distance of 25 mm corresponds to the upper end of distances recommended by the U.S. Federal Communications Commission when evaluating portable wireless devices while carried next to the body using suitable accessories [42].

As indicated earlier, the parameter of interest is the threshold power $P_{\mathrm{th},m}$, which is the transmit power level at which SAR_m evaluated at a transmit power of P_t has reached the SAR limit $\mathrm{SAR}_{\mathrm{limit},m}$. Thus

$$P_{\mathrm{th},m} = P_t \frac{\mathrm{SAR}_{\mathrm{limit},m}}{\mathrm{SAR}_m}. \tag{3}$$

Figs. 2 and 3 show the computed threshold power levels as functions of frequency at $s = 5$ mm for all dipole lengths under consideration (the y-axis of Figs. 2–5 uses a logarithmic scale). In Fig. 2, $P_{\mathrm{th,1g}}$ is given for $\mathrm{SAR}_{\mathrm{limit,1g}} = 1.6$ W/kg [2], and in Fig. 3, $P_{\mathrm{th,10\,g}}$ is given for $\mathrm{SAR}_{\mathrm{limit,10\,g}} = 2$ W/kg [3]. As expected, shorter antennas (i.e., narrower bandwidths) yield lower $P_{\mathrm{th},m}$. Also, $P_{\mathrm{th},m}$ decreases with increasing frequency partly due to the increase in tissue conductivity and partly due to the more localized energy loss for the shorter antennas. It is also observed that $P_{\mathrm{th},m}$ is generally more sensitive to antenna length at lower frequencies due to the shorter electrical distance between the antenna and the phantom, which results in increased antenna coupling.

In Figs. 4 and 5, the threshold power is plotted as a function of the antenna to phantom separation distance s for all antenna lengths under consideration. In Fig. 4, $P_{\mathrm{th,10\,g}}$ is given at 900 MHz for $\mathrm{SAR}_{\mathrm{limit,10\,g}} = 2$ W/kg, as 900 MHz is a commonly used frequency for cellular telephone service in countries that follow the ICNIRP guidelines. Likewise, since the 1900 MHz band is commonly used in North America where IEEE C95.1-1991 guidelines are followed, $P_{\mathrm{th,1g}}$ is given in Fig. 5. It can be seen from Figs. 4 and 5 that the logarithm

of $P_{\mathrm{th},m}$ varies almost linearly with distance s. Also, the relationship between $P_{\mathrm{th},m}$ and l/λ is predominantly linear at lower frequencies and logarithmic at higher frequencies. Thus, a simple mathematical relationship can be developed to estimate $P_{\mathrm{th},m}$ from these two variables at a given frequency. For instance, an equation of the form

$$\ln \hat{P}_{\mathrm{th},m} = As + B\ln(l/\lambda) + C(l/\lambda) + Ds\ln(l/\lambda) + E \tag{4}$$

can be applied, where $\hat{P}_{\mathrm{th},m}$ is an estimate of $P_{\mathrm{th},m}$ (in milliwatts), s is expressed in millimeters, and A, B, C, D, and E are frequency-dependent parameters. Parameters A and D are in units of $1/m$ and B, C, and E are unitless. The fourth term in (4) accounts for the interaction between the first two terms, as can be seen in Figs. 4 and 5. A least-squares fit of (4) to the $\mathrm{SAR}_{1\mathrm{g}}$ data yields values for A, B, C, D, and E that can be described by third-order polynomials of frequency, as shown in (5), where f is in gigahertz. The rms error of (4) and (5) to the $\mathrm{SAR}_{1\mathrm{g}}$ data is 8.7%:

$$\begin{bmatrix} 1000A \\ 100B \\ 10C \\ 1000D \\ 10E \end{bmatrix} = \begin{bmatrix} -9.67 & 43.9 & 1.49 & 4.48 \\ -8.01 & 69.4 & -194 & 185 \\ 3.18 & -23.6 & 52.7 & -11.6 \\ -2.47 & 10.8 & -8.63 & -21.2 \\ -3.33 & 27.4 & -79.3 & 90.8 \end{bmatrix} \begin{bmatrix} f^3 \\ f^2 \\ f \\ 1 \end{bmatrix}. \tag{5}$$

For $\mathrm{SAR}_{10\,\mathrm{g}}$, a least-squares solution of (4) with an rms error of 6.7% is given by

$$\begin{bmatrix} 1000A \\ 100B \\ 100C \\ 1000D \\ 10E \end{bmatrix} = \begin{bmatrix} -9.75 & 43.9 & -1.64 & 5.98 \\ -6.38 & 55.9 & -155 & 133 \\ 31.9 & -219 & 420 & -2.22 \\ -2.89 & 13.9 & -14.2 & -11.0 \\ -3.25 & 26.1 & -70.8 & 88.1 \end{bmatrix} \begin{bmatrix} f^3 \\ f^2 \\ f \\ 1 \end{bmatrix}. \tag{6}$$

Thus, simple and accurate formulas have been derived to determine the threshold power at any frequency, antenna length, and distance from the phantom within the ranges studied.

It is also interesting to observe how the absorption factor F_m and the radiation efficiency η_{rad} in (1) vary individually with the input variables and to see which behaviors dominate in determining $P_{\mathrm{th},m}$. Combining (1) and (3) yields an expression for $P_{\mathrm{th},m}$ as a function of η_{rad} and F_m

$$P_{\mathrm{th},m} = P_t \frac{\mathrm{SAR}_{\mathrm{limit},m}}{\mathrm{SAR}_m} = \frac{m\mathrm{SAR}_{\mathrm{limit},m}}{F_m(1-\eta_{\mathrm{rad}})} \tag{7}$$

where the values of F_m and η_{rad} both lie between 0 and 1. As explained earlier, the CENELEC EN 50371 standard gives a value of $P_{\mathrm{th},10\,\mathrm{g}} = 20$ mW for $\mathrm{SAR}_{\mathrm{limit},10\,\mathrm{g}} = 2$ W/kg, which is based on the overly conservative assumption that $F_{10\,\mathrm{g}} = 1$ and $\eta_{\mathrm{rad}} = 0$. These choices of $F_{10\,\mathrm{g}}$ and η_{rad} give the minimum value for $P_{\mathrm{th},10\,\mathrm{g}}$, and it was seen in Figs. 3 and 4 that $P_{\mathrm{th},10\,\mathrm{g}}$ can be much higher than 20 mW in practice, particularly at lower frequencies and larger distances from the phantom. The variation of $F_{10\,\mathrm{g}}$ and $1-\eta_{\mathrm{rad}}$ with frequency and antenna length is shown in Fig. 6 for $s = 5$ mm (the same case as in Fig. 3), whereas its variation with the separation distance and antenna length is reported in Fig. 7 for $f = 900$ MHz (the same case as in Fig. 4). The values of $1-\eta_{\mathrm{rad}} = P_{\mathrm{abs}}/P_t$ were

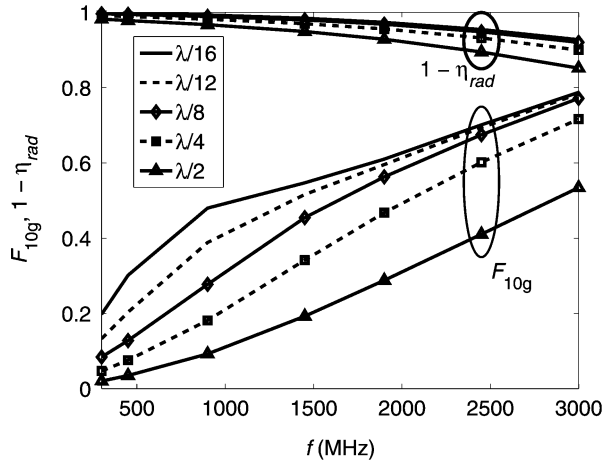

Fig. 6. $F_{10\,\mathrm{g}}$ and $1-\eta_{\mathrm{rad}}$ for $\mathrm{SAR}_{\mathrm{limit},10\,\mathrm{g}} = 2$ W/kg at $s = 5$ mm.

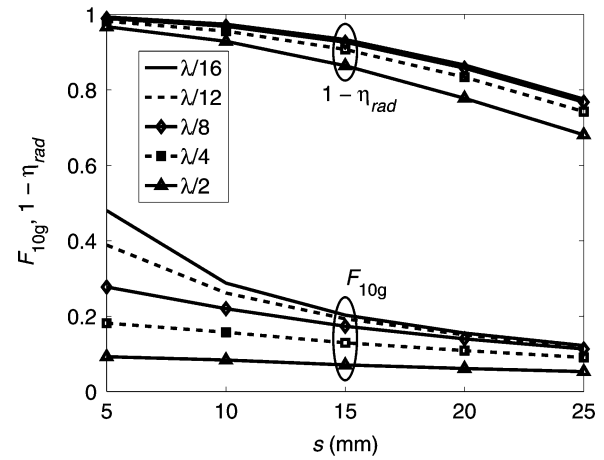

Fig. 7. $F_{10\,\mathrm{g}}$ and $1-\eta_{\mathrm{rad}}$ for $\mathrm{SAR}_{\mathrm{limit},10\,\mathrm{g}} = 2$ W/kg at $f = 900$ MHz.

calculated from radiated power $P_{\mathrm{rad}} = P_t - P_{\mathrm{abs}}$ and transmit power P_t, provided by the MoM simulations, and the values of $F_{10\,\mathrm{g}}$ were then calculated from (7), given that the other variables are known. For the dipole antenna setup studied in this paper, the SAR distributions have contour lines of equal SAR that are shaped like ellipses in the planes parallel to the phantom shell. The absorption factor F_m quantifies how concentrated the SAR distribution is about its peak (i.e., the spacing between the contour lines) with lower values of F_m corresponding to a more spread SAR distribution.

At lower frequencies, the radiation efficiency is very low, with nearly all of the transmitted power being absorbed in the phantom (see Fig. 6). This is due to the fact that the electrical distance of the antenna to the phantom s/λ is the smallest. However, $F_{10\,\mathrm{g}}$ is lowest at lower frequencies, resulting in higher $P_{\mathrm{th},m}$ values. This is because the absorbed power is spread over a larger volume in the phantom, partly due to the larger antenna sizes, resulting in greater spreading of the currents on the antenna, and partly due to the lower conductivity of the phantom material resulting in larger penetration depth; thus, there is less absorption near the exposed phantom surface. As the frequency increases, the radiation efficiency increases, but energy dissipation becomes more concentrated in the 10-g mass.

The data show that the variation of $P_{\mathrm{th},10\,\mathrm{g}}$ with frequency is predominantly influenced by $F_{10\,\mathrm{g}}$ and that $F_{10\,\mathrm{g}}$ and $1-\eta_{\mathrm{rad}}$ vary inversely with frequency. On the other hand, $F_{10\,\mathrm{g}}$ and $1-\eta_{\mathrm{rad}}$ vary similarly with antenna length, with shorter antennas having the largest values, and therefore, lowest $P_{\mathrm{th},10\,\mathrm{g}}$ values.

As the antenna is moved away from the phantom, the radiation efficiency improves, and the absorbed energy in the phantom becomes more spread, as expected (see Fig. 7). Both of these phenomena result in higher $P_{\mathrm{th},10\,\mathrm{g}}$ values at larger distances.

Overall, the data show that the radiation efficiency data can, in some cases, approach the $\eta_{\mathrm{rad}}=0$ assumption in CENELEC EN 50371 (at least for the conservative setup used here; the results for other setups will be discussed in the next section), but the absorption factor is typically far from the $F_{10\,\mathrm{g}}=1$ assumption. Incidentally, $F_{1\mathrm{g}}$ is significantly lower than $F_{10\,\mathrm{g}}$. The lower values of $F_{10\,\mathrm{g}}$ largely explain the higher $P_{\mathrm{th},10\,\mathrm{g}}$ values above 20 mW.

C. Comparison of Results With Other Findings

The objective of this section is to compare the results of the previous section with other findings in order to demonstrate that the results give conservative values for $P_{\mathrm{th},m}$, as discussed in Section I. This section consists of three parts:

1) a comparison of the radiation efficiency values discussed in the previous section with values found in the literature;
2) a comparison of the dipole results with the simulated results of a number of resonant antennas at 900 MHz;
3) a comparison of the dipole results with the measured results of portable wireless devices.

The radiation efficiencies for dipole antennas at 900 MHz in Fig. 7 range from 0.7 to 32%, with most values less than 20%. Okoniewski and Stuchly reported radiation efficiencies of a 915-MHz resonant monopole antenna on a box model of a portable wireless device next to different head models [9]. When a flat phantom was used, the radiation efficiency ranged from 16% at $s=15$ mm to 40% at $s=25$ mm. These results compare well with the radiation efficiency of the half-wavelength dipole in Fig. 7, which was 14–32% for same distances. The higher radiation efficiency of the monopole antenna may be due to the thickness of the box model that causes some currents on the device to be displaced away from the phantom. When two heterogeneous anatomical head models were used, Okoniewski and Stuchly reported radiation efficiencies ranging from 51% at $s=15$ mm to 73% at $s=25$ mm. These values are similar to the values for a homogeneous sphere reported by the same authors, and it was explained that the shape of the flat phantom is the main reason for it resulting in lower radiation efficiency, and thus, lower threshold power levels.

Others have also reported radiation efficiencies at 900 MHz for antennas mounted on a simple handset model and held against an anatomical head model. The reported radiation efficiencies are

- 22% and 29% for a meander monopole and a shorted patch, respectively [43];
- 19% and 25% for a helix and a monopole antenna, respectively [44];
- 44% and 54% for a monopole antenna and patch antenna, respectively (a hand model was also used to hold the device) [45];
- 47% and 32–52% for a monopole and three different PIFAs, respectively (a hand model was also used) [46].

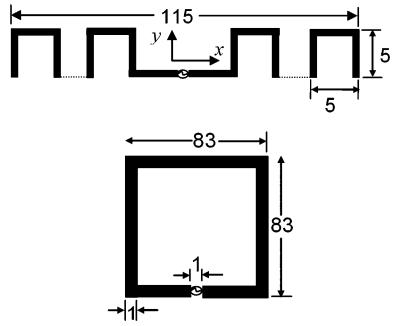

Fig. 8. Meander dipole and square-loop antennas under investigation (dimensions in millimeters).

TABLE VII
COMPARISON BETWEEN DIFFERENT ANTENNA TYPES AT $f=900$ MHZ AND $s=10$ MM

Antenna Type	BW_{7dB}	$P_{th,1g}$ (mW)	F_{1g}	$P_{th,10g}$ (mW)	F_{10g}	η_{rad}
Linear dipole	15.0%	117.6	1.5%	246.9	8.7%	6.6%
Meander dipole	12.7%	95.2	1.8%	202	10.5%	5.5%
λ/2.5 dipole	12.4%	101.0	1.7%	202	10.6%	6.2%
Square loop	7.0%	228.6	0.8%	465.1	4.7%	7.6%
λ/3.1 dipole	7.0%	79.3	2.1%	161.0	13.1%	5.2%

Since the handset is placed directly against the head model in these cases, these radiation efficiencies are compared against the dipole data for $s=5$ mm, which range from 0.7% to 3.2% for $l=\lambda/16$ to $\lambda/2$, respectively. This comparison indicates that the flat phantom and dipole antenna models used in this study give low values for radiation efficiency, resulting in conservative values for $P_{\mathrm{th},m}$.

To compare $P_{\mathrm{th},m}$ for 1-g and 10-g average SAR among other canonical antennas, we also considered three resonant antennas at 900 MHz: a strip dipole (1-mm wide strip infinitely thin and 155-mm long), a square-strip loop, and a meander dipole. The loop and meander dipole are shown in Fig. 8. All antennas are two-dimensional, which has the advantage that all parts of the antenna are at the same distance from the phantom. Computed impedance bandwidths of these three antennas at $s=10$ mm are shown in Table VII. The return loss was obtained with reference to a 50-Ω source. Table VII shows that, as expected, the bandwidth of the meander antenna is slightly narrower than the relatively long strip dipole. The narrow bandwidth of the loop antenna is due to its high resistance at resonance $(110\,\Omega)$.

Table VII compares the threshold powers, absorption factors, and radiation efficiencies for each of these antennas. When comparing between the strip and the meander dipoles, $P_{\mathrm{th},m}$ is clearly lower for the latter since its axial length is shorter (115 mm) than that of the strip dipole (155 mm). $P_{\mathrm{th},m}$ for the square-strip loop antenna is the highest among the three antennas because the SAR distribution from the loop has two separate

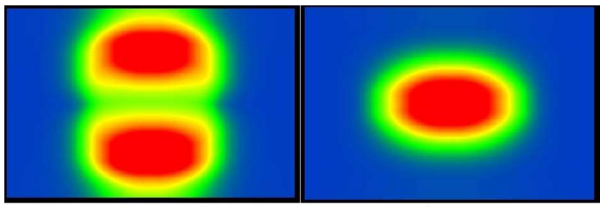

Fig. 9. Peak 1-g average SAR distributions. (a) Square-loop antennas. (b) Meander dipole antennas.

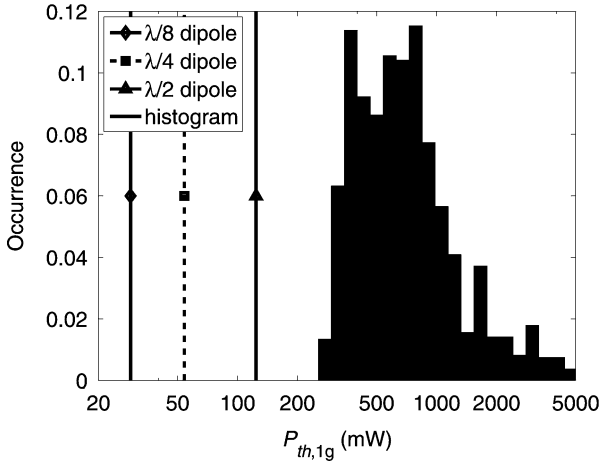

Fig. 10. Histogram of $P_{\mathrm{th,1g}}$ from 1344 SAR measurements of 54 portable wireless devices, compared with the computed $P_{\mathrm{th,1g}}$ values for dipole antennas of length $\lambda/8, \lambda/4$, and $\lambda/2$.

local maxima (see Fig. 9). For the meander dipole and square loop, the results are also shown next to data for linear dipoles with lengths that result in similar bandwidths. The threshold powers for the $\lambda/2.5$ dipole are very similar to the data for the meander dipole (within 6%), and the $\lambda/3.1$ dipole gives more conservative values for $P_{\mathrm{th},m}$ than does the square loop. This supports the use of thin-wire dipole antennas for the main part of this study.

The computed results of this paper are also compared with data from the measured SAR of portable wireless devices. A total of 1344 $\mathrm{SAR}_{1\mathrm{g}}$ measurements were taken from 54 products. The data are taken primarily from Motorola iDEN products, operating from 806 to 870 MHz, with an operating bandwidth requirement of 7.6%, as shown in Table IV. From Table III, it can be found that a dipole antenna of length no smaller than $\lambda/8$ will have a similar fractional bandwidth. We chose to examine the dipole antenna results for lengths of $\lambda/8, \lambda/4$, and $\lambda/2$. All measurements were taken with the devices held to the side of the head, so it makes sense to use a dipole antenna distance of $s = 5$ mm in the comparison. At a center frequency of 838 MHz, (4) and (5) yield $P_{\mathrm{th,1g}} = 29, 54$, and 124 mW for $l = \lambda/8, \lambda/4$, and $\lambda/2$, respectively. For the measured data, a histogram of $P_{\mathrm{th,1g}}$ of the portable wireless devices is shown in Fig. 10. The $P_{\mathrm{th,1g}}$ data are obtained by applying (3) to scale the measured transmit power P_t up by the ratio between $\mathrm{SAR}_{\mathrm{limit,1g}} = 1.6$ W/kg and the measured $\mathrm{SAR}_{1\mathrm{g}}$. It should be noted that there is a bias in the measured data, as they are from products that have been designed to be compliant with the SAR limits. However, the measured output power of the devices was typically 125 or 230 mW, both of which are less than the minimum of the $P_{\mathrm{th,1g}}$ values of the measured data, which is 256 mW. The calculated $P_{\mathrm{th,1g}}$ values for the three dipole antennas are significantly less than the measured $P_{\mathrm{th,1g}}$ values of all 54 portable wireless devices, further demonstrating that the calculated values of the power thresholds are conservative.

IV. Conclusion

The SAR characteristics of canonical antennas are investigated with the objective of estimating upper bounds for the transmit power of wireless communication devices demonstrating that the devices are inherently compliant with internationally accepted RF exposure limits. Simple expressions have been derived to estimate the threshold power levels over a wide range of dipole antenna lengths, frequencies, and distances from the phantom. Examples of meander and loop antennas are given to demonstrate the suitability of thin-wire dipole antennas in the study. Comparison of the simulated data with results from the literature and measurements of portable wireless devices has been used to demonstrate that the proposed approach gives conservative values for the threshold power. It is estimated that the maximum error of the calculations presented in this paper is on the order of 10%. Currently, further investigations are underway to extend this research to encompass other classes of antennas. The cost and complexity of compliance protocols could be possibly reduced if reasonable power thresholds for requiring SAR testing could be defined. This is an attempt in such a direction.

References

[1] C. K. Chou, H. Bassen, J. Osepchuk, Q. Balzano, R. Petersen, M. Meltz, R. Cleveland, J. C. Lin, and L. Heynick, "Radio frequency electromagnetic exposure: Tutorial review on experimental dosimetry," *Bioelectromagnetics*, vol. 17, no. 3, pp. 195–208, 1996.

[2] *IEEE Stand. for Safety Levels with Respect to Human Exposure to Radio Frequency Electromagnetic Fields, 3 kHz to 300 GHz*, IEEE Stand. C95.1-1991.

[3] ICNIRP, "International Commission on Non-Ionizing Radiation Protection guidelines for limiting exposure to time-varying electric, magnetic and electromagnetic fields (up to 300 GHz)," *Health Phys.*, vol. 74, no. 4, pp. 494–522, 1998.

[4] *IEEE Recommended Practice for Determining the Peak Spatial-Average Specific Absorption Rate (SAR) in the Human Head from Wireless Communication Devices: Measurement Techniques*, IEEE Stand. 1528-2003.

[5] *Human Exposure to Radio Frequency Fields from Hand-Held and Body-Mounted Wireless Communication Devices—Human Models, Instrumentation, and Procedures—Part 1: Procedure to Determine the Specific Absorption Rate (SAR) for Hand-Held Devices Used in Close Proximity to the Ear (Frequency Range of 300 MHz to 3 GHz)*, IEC Stand. 62209, Feb. 2005.

[6] K. S. Yee, "Numerical solution of initial boundary value problems involving Maxwell's equations in isotropic media," *IEEE Trans. Antennas Propag.*, vol. 14, no. 3, pp. 302–307, May 1966.

[7] R. F. Harrington, *Field Computation by Moment Methods*. New York: Macmillan, 1968.

[8] Q. Balzano, O. Garay, and T. J. Manning, "Electromagnetics energy exposure of simulated users of portable cellular telephones," *IEEE Trans. Veh. Technol.*, vol. 44, no. 3, pp. 390–403, Aug. 1995.

[9] M. Okoniewski and M. A. Stuchly, "A study of the handset antenna and human body interaction," *IEEE Trans. Microw. Theory Tech.*, vol. 44, no. 10, pp. 1855–1864, Oct. 1996.

[10] O. P. Gandhi, G. Lazzi, and C. Furse, "Electromagnetic absorption in the human head and neck for mobile telephones at 835 and 1900 MHz,"

IEEE Trans. Microw. Theory Tech., vol. 44, no. 10, pp. 1884–1897, Oct. 1996.
[11] G. Lazzi and O. P. Gandhi, "On modeling and personal dosimetry of cellular telephone helical antennas with the FDTD code," *IEEE Trans. Antennas Propag.*, vol. 46, no. 4, pp. 525–530, Apr. 1998.
[12] Q. Yu, O. P. Gandhi, M. Aronsson, and D. Wu, "An automated SAR measurement system for compliance testing of personal wireless devices," *IEEE Trans. Electromagn. Compat.*, vol. 41, no. 3, pp. 234–245, Aug. 1999.
[13] A. Drossos, V. Santomaa, and N. Kuster, "The dependence of electromagnetic energy absorption upon human head tissue composition in the frequency range 300–3000 MHz," *IEEE Trans. Microw. Theory Tech.*, vol. 48, no. 11, pp. 1988–1995, Nov. 2000.
[14] P. Bernardi, M. Cavagnaro, S. Pisa, and E. Piuzzi, "Power absorption and temperature elevations induced in the human head by a dual-band monopole-helix antenna phone," *IEEE Trans. Microw. Theory Tech.*, vol. 49, no. 12, pp. 2539–2546, Dec. 2001.
[15] S. Koulouridis and K. S. Nikita, "Study of the coupling between human head and cellular phone helical antennas," *IEEE Trans. Electromagn. Compat.*, vol. 46, no. 1, pp. 62–70, Feb. 2004.
[16] O. Kivekäs, J. Ollikainen, T. Lehtiniemi, and P. Vainikainen, "Bandwidth, SAR, and efficiency of internal mobile phone antennas," *IEEE Trans. Electromagn. Compat.*, vol. 46, no. 1, pp. 71–86, Feb. 2004.
[17] N. Kuster and Q. Balzano, "Energy absorption mechanism by biological bodies in the near field of dipole antennas," *IEEE Trans. Veh. Technol.*, vol. 41, no. 1, pp. 17–23, Feb. 1992.
[18] R. Y.-S. Tay, Q. Balzano, and N. Kuster, "Dipole configurations with strongly improved radiation efficiency for hand-held transceivers," *IEEE Trans. Antennas Propag.*, vol. 46, no. 6, pp. 798–806, Jun. 1998.
[19] S. Watanabe, M. Taki, T. Nojima, and O. Fujiwara, "Characteristics of the SAR distributions in a head exposed to electromagnetic fields radiated by a hand-held portable radio," *IEEE Trans. Microw. Theory Tech.*, vol. 44, no. 10, pp. 1874–1883, Oct. 1996.
[20] *Generic Standard to Demonstrate the Compliance of Low Power Electronic and Electrical Apparatus With the Basic Restrictions Related to Human Exposure to Electromagnetic Fields (10 MHz–300 GHz)—General Public*, CENELEC Stand. EN 50371, Nov. 2002.
[21] Remcom, Inc., State College, PA. (2006). XFDTD user's guide, version 6.3. [Online]. Available: http://www.remcom.com
[22] EM Software & Systems, Stellenbosch, South Africa. (2004, Oct.). FEKO user's manual, Suite 4.3. [Online]. Available: http://www.feko.info
[23] W. Kainz, A. Christ, T. Kellom, S. Seidman, N. Nikoloski, B. Beard, and N. Kuster, "Dosimetric comparison of the specific anthropomorphic mannequin (SAM) to 14 anatomical head models using a novel definition for the mobile phone positioning," *Phys. Med. Biol.*, vol. 50, pp. 3423–3445, Jul. 2005.
[24] B. Beard, W. Kainz, T. Onishi, T. Iyama, S. Watanabe, O. Fujiwara, J. Wang, G. Bit Babik, A. Faraone, J. Wiart, A. Christ, N. Kuster, A.-K. Lee, H. Kroeze, M. Siegbahn, J. Keshvari, H. Abrishamkar, W. Simon, D. Manteuffel, and N. Nikoloski, "Comparisons of computed mobile phone induced SAR in the SAM phantom to that in anatomically correct models of the human head," *IEEE Trans. Electromagn. Compat.*, vol. 48, no. 2, pp. 397–407, May 2006.
[25] *Human Exposure to Radio Frequency Fields from Handheld and Body-Mounted Wireless Communication Devices—Human Models, Instrumentation, and Procedures, Part 2: Procedure to Determine the Specific Absorption Rate (SAR) in the Head and Body for 30 MHz to 6 GHz Handheld and Body-Mounted Devices Used in Close Proximity to the Body*, Draft, IEC Stand. 62209, Feb. 2006.
[26] *IEEE Recommended Practice for Measurements and Computations of Radio Frequency Electromagnetic Fields With Respect to Human Exposure to Such Fields, 100 kHz–300 GHz*, IEEE Stand. C95.3-2002.
[27] M. Ali, "Miniaturized packaged (embedded) antennas for portable wireless devices," (invited paper), in *Encyclopedia of RF and Microw. Engineering*. Hoboken, NJ: Wiley, Feb. 2005, pp. 3068–3082.
[28] K. M. Z. Shams and M. Ali, "Study and design of a capacitively coupled polymeric internal antenna," *IEEE Trans. Antennas Propag.*, vol. 53, no. 3, pp. 985–993, Mar. 2005.
[29] M. Ali, T. Sittironnarit, H.-S. Hwang, R. A. Sadler, and G. J. Hayes, "Wideband/dual-band packaged antenna for 5–6 GHz WLAN application," *IEEE Trans. Antennas Propag.*, vol. 52, no. 2, pp. 610–615, Feb. 2004.
[30] M. F. Abedin and M. Ali, "Modifying the ground plane and its effect on planar inverted-F antennas (PIFAs) for mobile phone handsets," *IEEE Antennas Wireless Propag. Lett.*, vol. 2, no. 1, pp. 226–229, 2003.
[31] M. Ali, G. J. Hayes, H.-S. Hwang, and R. A. Sadler, "Design of a multi-band internal antenna for third generation mobile phone handsets," *IEEE Trans. Antennas Propag.*, vol. 51, no. 7, pp. 1452–1461, Jul. 2003.
[32] M. Ali, R. A. Sadler, and G. J. Hayes, "A uniquely packaged internal inverted-F antenna for bluetooth or wireless LAN application," *IEEE Antennas Wireless Propag. Lett.*, vol. 1, no. 1, pp. 5–7, 2002.
[33] M. Ali and G. J. Hayes, "A small printed integrated inverted-F antenna for bluetooth application," *Microw. Opt. Technol. Lett.*, vol. 33, no. 5, pp. 347–349, Jun. 2002.
[34] C. Di and Nallo and A. Faraone, "Multi-band internal antenna for mobile phones," *Electron. Lett.*, vol. 41, no. 9, pp. 514–515, Apr. 2005.
[35] L. J. Chu, "Physical limitations on omni-directional antennas," *J. Appl. Phys.*, vol. 19, pp. 1163–1175, Dec. 1948.
[36] H. A. Wheeler, "Small Antennas," *IEEE Trans. Antennas Propag.*, vol. AP-23, no. 4, pp. 462–469, Jul. 1975.
[37] R. C. Hansen, "Fundamental limitations of small antennas," *Proc. IEEE*, vol. 69, no. 2, pp. 170–182, Feb. 1981.
[38] J. S. McLean, "A re-examination of the fundamental limits on the radiation Q of electrically small antennas," *IEEE Trans. Antennas Propag.*, vol. 44, no. 5, pp. 672–676, May 1996.
[39] G. A. Thiele, P. L. Detweiler, and R. P. Penno, "On the lower bound of the radiation Q for electrically small antennas," *IEEE Trans. Antennas Propag.*, vol. 51, no. 6, pp. 1263–1269, Jun. 2003.
[40] W. Geyi, "A method for the evaluation of small antenna Q," *IEEE Trans. Antennas Propag.*, vol. 51, no. 8, pp. 2124–2129, Aug. 2003.
[41] D. M. Pozar, *Microwave Engineering*, 2nd ed. New York: Wiley, 1998, pp. 300–306.
[42] *Additional Information for Evaluating Compliance of Mobile and Portable Devices with FCC Limits for Human Exposure to Radio Frequency Emissions,* Federal Communications Commission OET Bull. 65 Suppl. C, Washington, DC, Jun. 2001.
[43] P. Vainikainen, J. Ollikainen, O. Kivekas, and K. Kelander, "Resonator-based analysis of the combination of mobile handset antenna and chassis," *IEEE Trans. Antennas Propag.*, vol. 50, no. 10, pp. 1433–1444, Oct. 2002.
[44] J. T. Rowley, R. B. Waterhouse, and K. H. Joyner, "Modeling of normal-mode helical antennas at 900 GHz and 1.8 GHz for mobile communications handsets using the FDTD technique," *IEEE Trans. Antennas Propag.*, vol. 50, no. 6, pp. 812–820, Jun. 2002.
[45] M. G. Douglas, M. Okoniewski, and M. A. Stuchly, "A planar diversity antenna for handheld PCS device," *IEEE Trans. Veh. Technol.*, vol. 47, no. 3, pp. 747–754, Aug. 1998.
[46] M. A. Jensen and Y. Rahmat Samii, "EM interaction of handset antennas and a human in personal communications," *Proc. IEEE*, vol. 83, no. 1, pp. 7–17, Jan. 1995.

Mohammod Ali (M'93–SM'03) received the B.Sc. degree in electrical and electronic engineering from Bangladesh University of Engineering and Technology, Dhaka, Bangladesh, in 1987 and the M.A.Sc. and Ph.D. degrees in electrical engineering from the University of Victoria, Victoria, BC, Canada, in 1994 and 1997, respectively.

He was with Bangladesh Institute of Technology, Chittagong, from 1988 to 1992. From January 1998 to August 2001, he was with Ericsson, Inc., Research Triangle Park, NC, first as a Staff Engineer and then as a Senior Staff Engineer. Since August 2001, he has been with the Department of Electrical Engineering, University of South Carolina, Columbia, where he is currently an Assistant Professor. He was also a Visiting Research Scientist with the Motorola Corporate EME Research Laboratory, Plantation, FL, from June to August 2004. He is the author or coauthor of more than 80 journal and conference publications and is the holder of five U.S. patents. His current research interests include miniaturized packaged (embedded) antennas, meta-materials and their antenna applications, distributed wireless sensors and rectennas, reconfigurable antennas, and portable/wearable antennas and their interactions with humans (SAR).

Dr. Ali is the recipient of the 2003 National Science Foundation Faculty Career Award and the 2006 College of Engineering and Information Technology Young Investigator Award from the University of South Carolina.

Mark G. Douglas (S'86–M'98–SM'05) received the B.Eng. and Ph.D. degrees from the University of Victoria, Victoria, BC, Canada, in 1990 and 1998, respectively, and the M.Sc. degree from the University of Calgary, Calgary, AB, Canada, in 1993, all in electrical engineering.

From 1998 to 2002, he was a Senior Technical Leader with the Antenna Development Group, Ericsson, Inc., Research Triangle Park, NC, and a member of the Ericsson EMF Research Group, Stockholm, Sweden, where he was engaged in antenna design and RF dosimetry. In 2002, he joined the Motorola Corporate EME Research Laboratory, Fort Lauderdale, FL, where he is currently a distinguished member of the Technical Staff. His current research interests include radio frequency dosimetry. He is the holder of five patents and has authored more than 20 refereed journal and conference papers.

Dr. Douglas is the Co-Chair of the IEEE International Committee on Electromagnetic Safety, Technical Committee 34, Subcommittee 2, and a contributing member of the International Electrotechnical Committee, Project Team 62209.

Abu T. M. Sayem (S'05) received the B.Sc. degree in electrical and electronic engineering from Bangladesh University of Engineering and Technology (BUET), Dhaka, Bangladesh, in 1999. He is currently working toward the Ph.D. degree in electrical engineering at the University of South Carolina, Columbia.

From February 2000 to October 2000, he was with Ekushey Television, Ltd., and from November 2000 to August 2003, he was an RF engineer at GrameenPhone, Ltd., Dhaka. His current research interests include miniature antennas, ultra wideband antennas, specific absorption rate (SAR), and bio-electromagnetics. He is the author or coauthor of several conference papers, journal articles, and one book chapter.

Antonio Faraone (M'97–SM'05) was born in Rome, Italy, in 1966. He received the *laurea* degree (*summa cum laude*) in electronics engineering and the Ph.D. degree in applied electromagnetics from the University of Rome "La Sapienza" in 1992 and 1997, respectively.

In 1997, he joined the Motorola Corporate EME Research Laboratory, Fort Lauderdale, FL, where he is currently the Manager of Portable Antenna Research and is engaged in theoretical and experimental research in antenna technologies and RF dosimetry. He is also actively involved in IEEE and IEC standards related to human exposure to electromagnetic energy. He is the holder of nine patents in antenna technology, with seven more pending, and has coauthored more than 20 refereed journal publications and 80 conference papers.

Chung-Kwang Chou (S'72–M'75–F'89) received the B.S.E.E. degree from the National Taiwan University, Taipei, Taiwan, R.O.C., in 1968, the M.S. degree from Washington University, St. Louis, MO, in 1971, and the Ph.D. degree from the University of Washington, Seattle, in 1975, all in electrical engineering.

He was a National Institutes of Health Postdoctoral Fellow in the Regional Primate Research Center and the Department of Physiology and Biophysics, University of Washington. He was an Assistant Professor from 1977 to 1981 and a Research Associate Professor from 1981 to 1985 in the Department of Rehabilitation Medicine and Center for Bioengineering, University of Washington. During 1985–1998, he was a Research Scientist and the Director of the Department of Radiation Research, City of Hope National Medical Center, Duarte, CA. In April 1998, he joined Motorola Florida Research Laboratory, Fort Lauderdale, where he is currently the Chief EME Scientist and the Director of the Corporate EME Research Laboratory, responsible for RF product safety. His current research interests include RF biological effects, RF dosimetry and exposure systems, and hyperthermia and electrochemical treatment of cancer. From 1987 to 2003, he was the Associate Editor of the *Journal of Bioelectromagnetics*.

Dr. Chou received the first special award in 1981 for the decade 1970–1979 from the International Microwave Power Institute, the outstanding paper award from the *Journal of Microwave Power* in 1985, the Curtis Carl Johnson Memorial Award for Preceptor of Best Student Poster from the Bioelectromagnetics Society in 1995, the IEEE Standards Medallion Award in 2005, and the d'Arsonval Medal from the Bioelectromagnetics Society in 2006. He was the Chairman of the IEEE/EMBS Committee on Man and Radiation during 1996–1997, the Co-Chairman of the IEEE Scientific Coordinating Committee 28, Subcommittee 4 on RF Safety Standard from 1997 to 2005, a member of the Board of Directors of the Bioelectromagnetics Society from 1981 to 1984, a distinguished Lecturer of the IEEE Engineering in Medicine and Biology Society during 1991–1992, and a Council Member of the NCRP from 1998 to 2004. Since 1990, he has been a member of the Electromagnetics Academy. Since 2005, he has been an Associate Member of the Motorola Science Advisory Board and, since 2001, the Science Adviser of the Mobile Manufacturers Forum. He has been a Fellow of the American Institute for Medical and Biological Engineering since 1996.